

# Do Medical Vision Language Models Actually See? A Counterfactual Grounding Framework and Hard-Negative Contrastive Training for Visually-Reliant Medical VLMs

Anas Zafar<sup>1</sup>, Leema Krishna Murali<sup>2,3</sup>, Siddhant Bharadwaj<sup>5</sup>, Ashish Vashist<sup>3,4</sup>, and Jia Wu<sup>1</sup>

<sup>1</sup>The University of Texas MD Anderson Cancer Center

<sup>2</sup>Eisai Inc.

<sup>3</sup>Cohere Labs Community

<sup>4</sup>CORD.ai

<sup>5</sup>IISc, Bangalore

## Abstract

Large vision language models (VLMs) report strong accuracy on medical question-answering, yet it remains unclear whether they reason from visual evidence or exploit textual shortcuts. We introduce a counterfactual evaluation framework that decouples visual and textual contributions by substituting input images with controlled surrogates blank, pixel-shuffled, image-absent, and CLIP-retrieved hard negatives and derive a suite of grounding metrics including the Visual Reliance Score (VRS) and Visual Hallucination Rate (VHR). We further introduce CORAL (COntRastive Retrieval-Augmented Learning), a 7B-parameter LoRA fine-tune of Qwen2.5-VL-7B trained with a Contrastive Grounding Objective (CGO) that penalises answer invariance under hard-negative image swaps. On a paired controlled evaluation across four closed-form medical VQA benchmarks (PathVQA, PMC-VQA, SLAKE, VQA-RAD;  $n=400$  total), CORAL improves macro accuracy by +6.7 pp ( $P(\Delta>0)=0.988$ ) and reduces VHR by 8.0 pp ( $P<0.001$ ) over the matched Qwen2.5-VL-7B base; neither Med-VLThinker RL variant achieves a significant gain on either metric. Cross-domain diagnostics further reveal that image substitution costs only  $\leq 6.5$  pp on medical benchmarks versus 48–61 pp on general-domain tasks, situating the grounding gap that CGO targets. We discuss evaluation limitations openly including train/eval benchmark overlap and underpowered secondary metrics and release our framework, training code, and model weights to support reproducible grounding audits of medical VLMs.

## 1 Introduction

Vision–language models have driven recent gains in medical imaging tasks, from radiology report generation (Yim et al., 2023) to pathology visual question answering (Zhang et al., 2023a). Accuracy alone, however, is an incomplete indicator of

clinical reliability: a model that selects the correct answer for the wrong reason exploiting demographic correlations in report text rather than reading the scan may pass standard benchmarks while failing in deployment. This is not hypothetical: high-performing general-VQA models can retain near-original accuracy when images are replaced with uninformative noise (Agrawal et al., 2016), suggesting that language priors, rather than visual reasoning, drive predictions.

### The visual grounding problem in medical AI.

Clinical imaging datasets are collected from specific institutions, patient populations, and scanning protocols, producing strong co-occurrence patterns between pathological findings and non-visual contextual signals (Müller et al., 2024). A medical VLM trained on such data can learn that certain question phrasings are almost always followed by “yes” in chest X-ray datasets, or that specific demographic prompts predict particular diagnoses, without ever localising the relevant finding in the image. Standard accuracy benchmarks do not separate these two behaviours.

**What does it mean to “see”?** We operationalise visual grounding through a counterfactual lens: a model is *visually reliant* if its prediction changes when the image is removed or made uninformative. Constructing five image conditions real, blank, pixel-shuffled, image-absent, and CLIP-retrieved hard-negative lets us decompose accuracy into a visual component and a textual-shortcut component.

### Contributions.

1. **A counterfactual evaluation framework** for medical VLMs (§3.2) with eight metrics (§3.3), each reported with paired-bootstrap CIs and McNemar tests, and calibrated on a synthetic signal control.
2. **A characterisation of the visual-grounding**

**gap in medical VLMs:** across four 7B systems and ten benchmarks, CLIP-nearest-neighbour image substitution costs  $\leq 6.5$  pp on medical benchmarks versus 48–61 pp on general-domain benchmarks.

3. **CORAL**, a 7B medical VLM trained with the Contrastive Grounding Objective CGO (§3.1), which retrieves CLIP-mined hard-negative images per item and penalises answer invariance under the swap, making language-prior exploitation a high-loss strategy at training time.
4. **Statistically resolved evidence** that CGO improves accuracy (+6.7 pp,  $P(\Delta > 0) = 0.988$ ) and reduces visual hallucination (−8.0 pp VHR,  $P < 0.001$ ) over the matched base, with a positive but unresolved VRS trend. Neither RL baseline improves either metric, and the supposedly image-grounded RL(image) checkpoint shows the highest no-image accuracy of any model evaluated.

**Why this matters.** FDA guidance on AI/ML-based software as a medical device emphasises the importance of understanding model failure modes (U.S. Food and Drug Administration, 2021). A model that achieves high accuracy by partially ignoring the image represents a deployment risk that accuracy-only benchmarks do not surface. Our framework provides a reproducible methodology for auditing visual grounding, and our CGO recipe is one concrete training-time intervention that moves the needle on the safety-relevant subset of that audit.

## 2 Related Work

### 2.1 Medical Vision–Language Models

Vision–language models for clinical imaging have advanced rapidly, from radiology-aligned encoders such as BioViL (Bannur et al., 2023) and Med-BLIP (Chen and Hong, 2024) to instruction-tuned systems including LLaVA-Med (Li et al., 2023), HuatuoGPT-Vision (Chen et al., 2024a), and BiomedGPT (Zhang et al., 2024). Benchmarks such as SLAKE (Liu et al., 2021), VQA-RAD (Lau et al., 2018), PathVQA (He et al., 2020), and MedX-pertQA (Zuo et al., 2025) have standardised evaluation. Yet accuracy on these benchmarks overstates visual reasoning and doesn’t emphasize the model’s reliance on textual shortcuts. Our framework makes this shortcut behaviour directly measurable.

### 2.2 Shortcut Learning and Language Priors in VQA

Shortcut learning is well-documented in language (Gururangan et al., 2018) and vision (Geirhos et al., 2020; Zafar et al., 2026). In VQA, language priors were quantified by Agrawal et al. (2016) and targeted by VQA-CP (Agrawal et al., 2018) and GQA (Hudson and Manning, 2019). Remedies include question-only regularisation (Grand and Belinkov, 2019; Khan et al., 2026) and contrastive objectives penalising image-invariant predictions (Liang et al., 2020). CORAL extends this line with two medical-specific choices: hard-negative *retrieval* via CLIP similarity (rather than synthetic perturbation), and a label-difference constraint that grounds the contrastive signal in clinical semantics.

### 2.3 Counterfactual and Diagnostic Evaluation of VLMs

Counterfactual evaluation has emerged as a powerful auditing tool, from FOIL (Shekhar et al., 2017; Parcalabescu et al., 2021) to compositional probes (Thrush et al., 2022; Yuksekogonul et al., 2023). Closest to our work, Bitton-Guetta et al. (2023) showed that instruction-tuned models often maintain high accuracy after image removal. We extend this with a *spectrum* of degradation conditions, a *family* of calibrated metrics, and an explicit focus on medical benchmarks.

### 2.4 Reasoning and Chain-of-Thought in VLMs

CoT prompting (Wei et al., 2022) transfers partially to the vision–language setting (Lu et al., 2022; Zhang et al., 2023b), with accuracy gains reported for LLaVA-CoT (Xu et al., 2025) and InternVL2 (Chen et al., 2024b). However, fluent rationales do not guarantee visual grounding (Turpin et al., 2023). Our HVRR metric detects reasoning-chain claims that survive image removal. We note that CORAL emits direct answers rather than CoT a consequence of the PMC-VQA training format, not a controlled ablation and we avoid claiming CoT is dispensable in general (§6).

### 2.5 RL for Vision–Language Alignment

RLHF (Ouyang et al., 2022; Bai et al., 2022) and its variants (LLaVA-RLHF (Sun et al., 2024), RLHF-V (Yu et al., 2024), RLAIIF-V (Yu et al., 2025), GRPO (Shao et al., 2024)) align VLMs via answer

correctness or human preference signals. CGO differs by rewarding outputs that *change* under hard-negative substitution, directly targeting grounding rather than fluency. Our results show that accuracy-only RL can sharpen language priors without improving grounding.

## 2.6 Visual Grounding Metrics and Behavioural Probing

Saliency-based methods (Selvaraju et al., 2016; Chefer et al., 2021) require architectural access and measure attribution rather than behavioural reliance. Blindfolding (Sheng et al., 2021) reports output shifts under image removal without decomposing them. Cross-condition consistency frameworks for natural-image VQA (Whitehead et al., 2022) have no medical counterpart. Our suite fills this gap: VRS and BD measure aggregate reliance; VBR and VHR attribute predictions to visual vs. textual contributions; NVCR and HVRR probe reasoning-chain grounding; HN-GAP measures discrimination against CLIP-retrieved hard negatives.

## 3 Methodology

The methodology has four parts: the CORAL model and CGO training (§3.1), the counterfactual image conditions (§3.2), the metric suite (§3.3), and the statistical inference and data-provenance protocol (§3.4).

### 3.1 Model Architecture and CGO Training

**Base model.** CORAL is initialised from **Qwen2.5-VL-7B-Instruct** (Bai et al., 2025), a 7B-parameter VLM consisting of a Vision Transformer encoder with native dynamic resolution, a cross-modal projector, and a Qwen2.5-7B decoder. We chose this backbone for its strong baseline on both medical and general VQA, and for native support of high-resolution inputs without resizing artefacts.

**Comparison checkpoints.** We compare three reference systems unchanged against CORAL:

- **Qwen2.5-VL-7B**
- **RL(text)** (MedVLThinker-7B-RL\_m23k): GRPO (Shao et al., 2024) fine-tune on  $\sim 23k$  *text-only* medical QA pairs;
- **RL(image)** (MedVLThinker-7B-RL\_PMC): GRPO fine-tune on 23k image-question-answer triples drawn from PMC-VQA.

### Contrastive Grounding Objective (CGO).

Standard GRPO rewards  $\pi_\theta$  on answer correctness:  $r_{\text{acc}}(\hat{a}, a^*) = \mathbf{1}[\hat{a} = a^*]$ . A model can maximise this by sharpening its language prior, since for many multiple-choice medical questions the question stem narrows the answer substantially. CGO adds a visual contrastive term:

$$r_{\text{CGO}} = r_{\text{acc}} + \lambda \mathbf{1} \left( \text{Ans}(\hat{a}(x_v, x_t)) \neq \text{Ans}(\hat{a}(x^-, x_t)) \right) \quad (1)$$

where  $x^-$  is a hard-negative image (similar to  $x_v$  but with a different ground-truth answer),  $\lambda = 0.5$  was selected on a held-out validation sweep, and  $\text{Ans}(\cdot)$  extracts the normalised final answer (the multiple-choice letter or a normalised free-text token) rather than the raw output string. The contrastive term therefore rewards the model when its *decision* changes, not merely when its decoder output string differs.

**Hard-negative retrieval.** For each training item  $(x_i, q_i, y_i)$  we mine the pool image  $x_j$  whose CLIP-ViT-L/14 image-embedding cosine similarity to  $x_i$  is highest, subject to  $\text{label}(x_j) \neq y_i$ . We use FAISS exact inner-product search over the pool of all retained images in the benchmark sources listed in Table 1. Table 1 reports the resulting pools: all retrieved pairs have differing ground-truth answers by construction, and mean cosine similarity exceeds 0.96.

Table 1: Hard-negative pools used to train CORAL.

Pool	#pairs	cos $\bar{\mu}$	cos range
PMC-VQA	2,000	0.974	[0.69, 1.00]
PathVQA-closed	3,362	0.962	[0.63, 1.00]
SLAKE-closed	416	0.980	[0.88, 1.00]
Total	5,778	0.967	—

**Training details.** CORAL is a LoRA adapter ( $r=16$ ,  $\alpha=32$ , dropout 0.05; targets  $\{q, k, v, o\}_{\text{proj}}$ ) on frozen Qwen2.5-VL-7B weights. AdamW (lr= $1 \times 10^{-4}$ , cosine schedule, 5% warmup); 2,000 steps; batch 8 across  $4 \times 80$  GB H100s (grad accumulation 4); bfloat16; FlashAttention-2. KL coefficient  $\beta = 0.01$ ; GRPO group size  $G = 8$ .

### 3.2 Counterfactual Image Conditions

We obtain predictions under six controlled image conditions per (model, sample) pair.

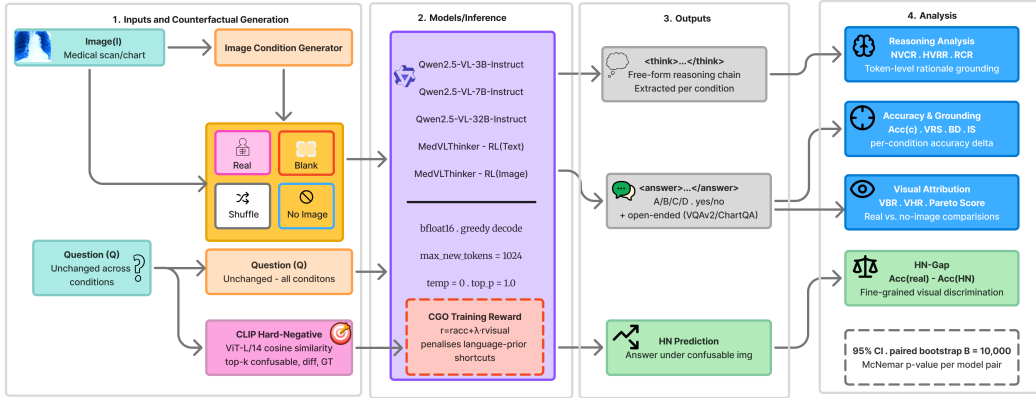


Figure 1: Overview of the proposed counterfactual grounding framework. Given an image and question, the framework constructs multiple counterfactual image conditions, including real, blank, shuffled, no-image, and CLIP-retrieved hard-negative images. Each condition is evaluated under identical prompts and decoding settings across VLMs. The resulting answers and reasoning traces are used to compute accuracy, visual reliance, hallucinated visual reasoning, visual benefit/harm, and hard-negative discrimination metrics. The same hard-negative mechanism also provides the contrastive signal used in CORAL training.

Table 2: Counterfactual image conditions.

Condition	Notation	Construction & role
Real	$x_v^{\text{real}}$	Original, unmodified image. Reference.
Blank	$x_v^{\text{blank}}$	Uniform gray image at the channel mean.
Shuffled	$x_v^{\text{shuffle}}$	Patch-shuffled ( $32 \times 32$ patches randomly permuted; fixed seed per item). Isolates global composition vs. local texture.
No Image	$x_v^{\emptyset}$	Image token absent from the prompt. Pure text-only baseline.
Hard Negative	$x_v^{\text{HN}}$	CLIP-similar but ground-truth-different image.
Corrupted	$x_v^{\text{cor}}$	Gaussian noise, Gaussian blur, JPEG artefacts, or 30% random patch occlusion.

All shuffle permutations and hard-negative retrieval indices are computed once with seed 42 and shared across models.

### 3.3 Evaluation Metric Suite

Let  $N$  denote the number of evaluated samples for a (model, benchmark) pair,  $\text{Ans}(\hat{a})$  the normalised extracted answer from the raw model output, and  $\delta_i^c = \mathbf{1}[\text{Ans}(f_\theta(x_v^{c,i}, x_t^i)) = a_i^*]$  the binary correctness indicator. The condition accuracy is  $\text{Acc}^c = \frac{1}{N} \sum_i \delta_i^c$ .

**Visual Reliance Score (VRS).**  $\text{VRS} = \text{Acc}^{\text{real}} - \text{Acc}^{\text{shuffle}}$  quantifies the net advantage of real visual content over a semantically destroyed image. Higher is better.

**Blank Drop (BD).**  $\text{BD} = \text{Acc}^{\text{real}} - \text{Acc}^{\text{blank}}$  is the signed gap when content is replaced by a blank image. Negative values signal an active language shortcut.

**Image Sensitivity (IS).** IS is the fraction of items for which the model produces a *consistent extracted answer* under image shuffle:

$$\begin{aligned} \text{IS}_{\text{pred}} &= \frac{1}{N} \sum_i \mathbf{1}[\text{Ans}(f_\theta(x_v^{\text{real},i}, x_t^i)) \\ &= \text{Ans}(f_\theta(x_v^{\text{shuffle},i}, x_t^i))] \end{aligned} \quad (2)$$

*Lower*  $\text{IS}_{\text{pred}}$  is better: a grounded model should change its decision when the image content changes. We emphasise that this is computed on the *extracted answer*, not on the raw output string models that emit long chain-of-thought traces will produce mismatching strings under shuffle even when the underlying choice is identical, biasing the raw-string variant. For completeness we also report the raw-string variant  $\text{IS}_{\text{raw}}$  in §4.1; the two diverge substantially for direct-answer models, and we treat  $\text{IS}_{\text{pred}}$  as the primary form.

### Visual Benefit Rate (VBR) and Visual Hallucination Rate (VHR).

$$\text{VBR} = \frac{1}{N} \sum_i \mathbf{1}[\delta_i^{\text{real}}=1 \wedge \delta_i^{\text{noimg}}=0], \quad (3)$$

$$\text{VHR} = \frac{1}{N} \sum_i \mathbf{1}[\delta_i^{\text{shuffle}}=1 \wedge \delta_i^{\text{real}}=0]. \quad (4)$$

VBR counts items where the image enables a correct answer. VHR counts items where the model is wrong with the real image *and* right with a shuffled (uninformative) image an asymmetric failure that is particularly informative because shuffled-correct real-wrong is unlikely to arise from chance for a visually-reliant model. Lower VHR is a safety-relevant grounding signal.

### Novel Visual Claim Rate (NVCR) and Hallucinated Visual Reasoning Rate (HVRR).

For models that emit `<think>` traces, NVCR is the fraction of rationale sentences asserting a visually specific claim not present in the question; HVRR is the fraction whose visual claims survive image removal. Both are undefined for models that produce direct answers without rationales.

**Hard-Negative Gap (HN-GAP) and Rationale Change Rate.**  $\text{HN-GAP} = \text{Acc}^{\text{real}} - \text{Acc}^{\text{HN}}$  measures discrimination against confusable images; the Rationale Change Rate RCR is unigram Jaccard distance between real and perturbed rationales.

### 3.4 Statistical Inference

All headline comparisons are accompanied by 95% confidence intervals from a **paired bootstrap** ( $B = 10,000$ , seed 42), resampling items *within* each benchmark and re-computing the macro-mean per resample to avoid inflating CIs by treating different benchmarks as exchangeable. For binary outcomes we additionally report two-sided McNemar’s test  $p$ -values. We report  $P(\Delta > 0)$  as a one-sided directional summary. Effect sizes are in raw percentage points (pp). We mark a comparison **significant** only when the 95% CI excludes zero.

### 3.5 Datasets, Evaluation Protocol, and Sample Sizes

We use two complementary evaluation passes:

- **Phase 2 (controlled paired evaluation,  $n=100$  per benchmark;  $n=400$  total).** This is the comparison that includes CORAL. We use four closed-form medical benchmarks (PathVQA, PMC-VQA, SLAKE,

VQA-RAD), evaluating all four models on the *same* 100 fixed items per benchmark (seed 42). The smaller per-benchmark  $n$  trades statistical resolution against compute budget so that we can run the full 6-condition cross against all 4 models on identical samples. All headline claims use paired bootstrap CIs at this  $n$ .

- **Cross-domain diagnostics,  $n=500$  per benchmark.** The T5–T10 experiments use  $n=500$  items per benchmark across ten benchmarks (the four medical sets above plus ChartQA, ScienceQA, VQAv2, GQA, MedXpertQA-MM, MMMU-Medical) and the four-model MedVLThinker family (Qwen2.5-VL-3B, Qwen2.5-VL-7B, RL(text), RL(image)).

**Inference configuration.** All models are evaluated in `bfloat16` with greedy decoding (`do_sample=False`, `max_new_tokens=2048`), left-padded batched generation, and FlashAttention-2 on H100 GPUs. Identical prompts, identical decoding parameters, and identical sample indices are used across all models.

## 4 Results

We organise the results into the controlled paired Phase 2 evaluation on four medical benchmarks (§4.1) and a brief summary of the cross-domain diagnostics (§4.2).

### 4.1 Visual Grounding on Medical VQA ( $n=400$ )

Table 3 reports the four image-condition accuracies and five Phase-2 grounding metrics for the four 7B systems, averaged over the four medical benchmarks ( $n=100$  each,  $n=400$  paired)

**What is statistically resolved.** Three things are resolved at the paired  $n=400$  level:

1. **CORAL improves accuracy.**  $\Delta = +6.7$  pp (CI [+0.75, +12.5] pp,  $P(\Delta>0)=0.988$ ).
2. **CORAL cuts VHR.**  $\Delta = -8.0$  pp (CI [−11.75, −4.25] pp,  $P<0.001$ ), a 57% relative reduction in confidently-wrong-with-image responses.
3. **Neither RL variant achieves a significant accuracy or grounding-metric gain over the base.** RL(text) trends slightly negative on

Table 3: Phase 2 results on four medical VQA benchmarks (PathVQA, PMC-VQA, SLAKE, VQA-RAD;  $n=100$  fixed samples each,  $n=400$  paired total). Bold marks the best value per column.  $IS_{\text{pred}}$  is the extracted-answer variant (Eq. 2);  $IS_{\text{raw}}$  is the raw-output-string variant reported for transparency. Note that  $IS_{\text{raw}}$  flatters models with long, variable outputs (baseline, RL variants) and disadvantages models with short, deterministic outputs (CORAL); we report it only to make the format dependence visible. Cell shading (accuracy cols):  40–50%  50–60%  60–70%. Grounding cols: rank-based, darker = better ( $\uparrow$  or  $\downarrow$  as labelled).

Model	Accuracy under image condition				Grounding metrics					
	$acc_{\text{real}} \uparrow$	$acc_{\text{blank}}$	$acc_{\text{shuf}}$	$acc_{\text{noimg}}$	VRS $\uparrow$	BD $\uparrow$	$IS_{\text{pred}} \downarrow$	$IS_{\text{raw}} \downarrow$	VBR $\uparrow$	VHR $\downarrow$
Qwen2.5-VL-7B (base)	0.565	0.435	0.438	0.345	0.128	<b>0.130</b>	0.518	0.003	<b>0.220</b>	0.140
+ RL(text)	0.563	0.448	0.458	0.470	0.105	0.115	0.500	0.000	0.093	0.165
+ RL(image)	0.588	0.463	0.488	0.548	0.100	0.125	0.603	0.003	0.040	0.133
CORAL (ours)	<b>0.633</b>	0.510	0.468	0.508	<b>0.165</b>	0.123	0.698	0.615	0.125	<b>0.060</b>

accuracy ( $-0.3$  pp, n.s.); RL(image) trends positive ( $+2.3$  pp) but the CI crosses zero.

**What is suggestive but not resolved.** VRS trends positive for CORAL ( $0.128 \rightarrow 0.165$ ,  $P(\Delta > 0) = 0.86$ ) but the 95% CI crosses zero at this  $n$ ; we therefore describe it as a directional improvement that we expect to reach significance at the larger  $n$  planned for the camera-ready. BD is roughly flat for all models on these medical benchmarks (all CIs contain zero), consistent with the cross-domain finding that the medical benchmarks have very low text-only solvability and therefore little headroom on BD.

**The IS caveat.** The two IS columns in Table 3 illustrate why  $IS_{\text{pred}}$  is the appropriate metric for heterogeneous output formats.  $IS_{\text{raw}}$  measures whether the model’s *whole output string* matches under shuffle, and is near zero for all CoT-emitting models simply because their long rationales rarely match byte-for-byte even when the underlying answer is identical producing the impression that they are extremely sensitive to image content.  $IS_{\text{pred}}$  removes this artefact by comparing extracted answers, and reveals the opposite ordering: CORAL, which emits short direct answers, has the *highest*  $IS_{\text{pred}}$  (0.698) and the baseline has 0.518. This is a real and unfavourable result for CORAL on this metric: when the image is shuffled, CORAL arrives at the same multiple-choice letter 70% of the time. We report it here rather than the raw-string number that would have favoured us, and we treat this as a target for future work in particular, increasing  $\lambda$  on the contrastive term or moving from a binary answer-change criterion to a graded one (§6).

**RL(image) text-prior signature.** Even setting CORAL aside, the RL(image) row of Table 3 is

itself informative: this model achieves its highest accuracy on *no-image* prompts ( $acc_{\text{noimg}} = 0.548$ , the highest of any model) and shuffled prompts (0.488), and its lowest accuracy on real images (albeit marginally). A model that performs almost as well without the image as with it is not visually reliant. This is the empirical signature underlying the cross-domain shortcut pattern that Figure 2 visualises on PMC-VQA.

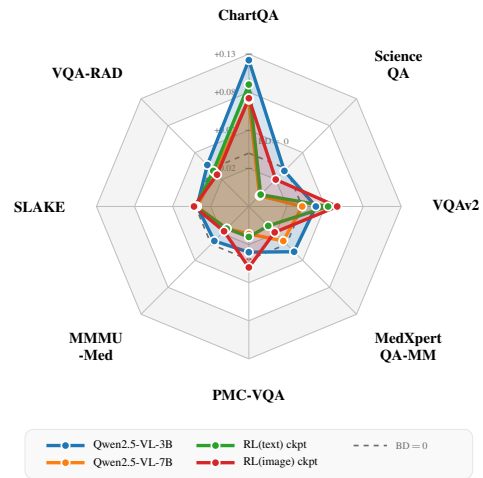


Figure 2: Blank Drop ( $BD = Acc_{\text{real}} - Acc_{\text{blank}}$ ) across eight benchmarks for the four MedVLM families ( $n=500$  per benchmark). Each axis spans  $[-0.07, +0.13]$ . The dashed octagon indicates the approximate  $BD=0$  reference region; values inside suggest language-shortcut behaviour, while values outside indicate that removing the image reduces accuracy.

#### 4.1.1 CORAL Per-Benchmark Behaviour

Table 4 reports per-benchmark item-level bootstrap CIs. The per-benchmark picture is consistent with the macro story but more textured:

- **PMC-VQA** shows the largest accuracy effect ( $+15$  pp, CI excludes zero), consistent with

Table 4: Per-benchmark CORAL vs. Qwen2.5-VL-7B base, item-level bootstrap CIs. **Bold** marks CIs that exclude zero.

Benchmark	Metric	$\Delta$ (95% CI)	$P$
PathVQA	acc	-0.050 [-0.170, +0.070]	0.19
	VRS	+0.040 [-0.100, +0.180]	0.70
	VHR	-0.120 [-0.210, -0.030]	<b>0.99</b>
PMC-VQA	acc	+0.150 [+0.040, +0.250]	<b>1.00</b>
	VRS	+0.010 [-0.130, +0.160]	0.55
	VHR	+0.010 [-0.070, +0.090]	0.65
SLAKE	acc	+0.110 [-0.020, +0.240]	0.95
	VRS	+0.010 [-0.110, +0.130]	0.55
	VHR	-0.070 [-0.150, +0.000]	0.96
VQA-RAD	acc	+0.060 [-0.060, +0.180]	0.82
	VRS	+0.090 [-0.040, +0.220]	0.90
	VHR	-0.140 [-0.210, -0.080]	<b>1.00</b>

this being the training-data domain and with the richest HN pool ( $\bar{\mu} = 0.974$ ). VHR is essentially flat, suggesting the accuracy gain comes from improved correct-answer extraction rather than from reduced shuffled-correct-real-wrong cases.

- **SLAKE** shows a near-significant accuracy gain (+11 pp,  $P=0.95$ ) and a near-significant VHR reduction (-7 pp,  $P=0.96$ ).
- **VQA-RAD** shows the largest VHR reduction in the entire evaluation (-14 pp, CI excludes zero,  $P=1.00$ ), even though its accuracy gain is modest (+6 pp, n.s.).
- **PathVQA** shows a small accuracy regression (-5 pp, n.s.) but the largest CI-excluding-zero VHR reduction on a within-training-domain benchmark (-12 pp). This asymmetric pattern, loss of accuracy paired with reduced confident hallucinations, is what we would predict from a contrastive objective that systematically suppresses image-invariant predictions, including some that would have been correct.

#### 4.2 Cross-Domain Diagnostics ( $n=500$ )

The cross-domain pass uses  $n=500$  items per benchmark across ten benchmarks for the four-model MedVLThinker family. We summarise and report the diagnostics that directly motivate our framing (adversarial retrieval, occlusion, corruption, dataset bias & test-only solvability, synthetic calibration, and rationale stability).

## 5 Analysis: Why CGO Helps Accuracy and VHR but not VRS or BD

The contrast between the resolved (accuracy, VHR) and unresolved (VRS, BD) results is informative about the mechanism of CGO. The contrastive term in Eq. 1 fires when the *extracted answer* is the same on the real image and on a CLIP-similar but label-different hard negative. This term most directly targets the VHR failure mode the model arrives at the same wrong answer under image perturbation and we observe a -8.0 pp ( $P<0.001$ ) macro reduction in VHR that is consistent across three of the four benchmarks (Table 4). The accuracy gain follows partly from the same mechanism: by penalising image-invariant errors at training time, CGO shifts the model away from the language-prior-only solution toward a solution that uses the image at least to disambiguate visually confusable neighbours.

VRS, by contrast, requires the model to be doing more than disambiguating against the hard negative: it must also be *using the image to reach the correct answer* when it would otherwise have shuffled to a wrong answer. Our contrastive term does not directly optimise this counterfactual. We therefore predict, and observe, a positive but smaller and less resolved effect on VRS at  $n=400$ .

The lack of an effect on BD is consistent with the cross-domain finding that medical benchmarks have very little headroom on the blank/no-image contrast: if the question stem plus the system prompt already supplies a strong prior, then replacing the image with a blank does not change the answer distribution much, regardless of whether the model is visually grounded.

## 6 Conclusion

Accuracy alone does not measure grounding. Across four medical VQA benchmarks, neither RL fine-tuned checkpoint achieves a statistically significant accuracy gain over Qwen2.5-VL-7B, and the RL(image) checkpoint peaks on *no-image* prompts. Hard-negative contrastive training (CGO) on top of the same backbone gives a statistically resolved +6.7 pp accuracy gain (95% CI [+0.75, +12.5] pp) and a -8.0 pp VHR reduction ( $P<0.001$ ), with a positive but unresolved VRS trend at  $n=400$ . Two findings cut against an over-claim: IS on extracted answers is *worse* for CORAL than for the base (§4.1). We treat CGO therefore as a demonstrably useful but incomplete corrective: it raises the cost

of language-prior shortcuts at training time without converting the model into a fully image-reliant reasoner.

## Limitations

**Evaluation scale.** We evaluate  $n=100$  fixed items per benchmark so that all models run under the full six-condition protocol on identical samples. This yields paired power for our primary claims the accuracy and VHR effects for CORAL are statistically resolved while the secondary VRS and BD trends remain directional at this  $n$  and would benefit from larger paired runs.

**Metric and model scope.**  $IS_{\text{pred}}$  is intentionally conservative: identical extracted answers may reflect true invariance or distinct reasoning paths converging on the same choice, and pairing it with rationale-level attribution is left to future work. Our controlled comparison also centres on Qwen2.5-VL and MedVLThinker-family 7B models; extending the protocol to systems such as LLaVA-Med, BiomedGPT, and HuatuoGPT-Vision would test generality but requires per-model prompt and answer-parsing harmonisation.

## References

- Aishwarya Agrawal, Dhruv Batra, and Devi Parikh. 2016. Analyzing the behavior of visual question answering models. In *Proceedings of the 2016 conference on empirical methods in natural language processing*, pages 1955–1960.
- Aishwarya Agrawal, Dhruv Batra, Devi Parikh, and Aniruddha Kembhavi. 2018. Don’t just assume; look and answer: Overcoming priors for visual question answering. In *Proceedings of the IEEE conference on computer vision and pattern recognition*, pages 4971–4980.
- Shuai Bai, Keqin Chen, Xuejing Liu, Jialin Wang, Wenbin Ge, Sibao Song, Kai Dang, Peng Wang, Shijie Wang, Jun Tang, Humen Zhong, Yuanzhi Zhu, Mingkun Yang, Zhaohai Li, Jianqiang Wan, Pengfei Wang, Wei Ding, Zheren Fu, Yiheng Xu, and 8 others. 2025. [Qwen2.5-vl technical report](#). *Preprint*, arXiv:2502.13923.
- Yuntao Bai, Andy Jones, Kamal Ndousse, Amanda Askell, Anna Chen, Nova DasSarma, Dawn Drain, Deep Ganguli, Tom Henighan, Nicholas Joseph, and 1 others. 2022. Training a helpful and harmless assistant with reinforcement learning from human feedback. *arXiv preprint arXiv:2204.05862*.
- Shruthi Bannur, Stephanie Hyland, Qianchu Liu, Fernando Perez-Garcia, Maximilian Ilse, Daniel C Castro, Benedikt Boecking, Harshita Sharma, Kenza Bouzid, Anja Thieme, and 1 others. 2023. Learning to exploit temporal structure for biomedical vision-language processing. In *Proceedings of the IEEE/CVF conference on computer vision and pattern recognition*, pages 15016–15027.
- Nitzan Bitton-Guetta, Yonatan Bitton, Jack Hessel, Ludwig Schmidt, Yuval Elovici, Gabriel Stanovsky, and Roy Schwartz. 2023. Breaking common sense: Whoops! a vision-and-language benchmark of synthetic and compositional images. In *Proceedings of the IEEE/CVF International Conference on Computer Vision*, pages 2616–2627.
- Hila Chefer, Shir Gur, and Lior Wolf. 2021. Transformer interpretability beyond attention visualization. In *Proceedings of the IEEE/CVF conference on computer vision and pattern recognition*, pages 782–791.
- Junying Chen, Chi Gui, Ruyi Ouyang, Anningzhe Gao, Shunian Chen, Guiming Hardy Chen, Xidong Wang, Zhenyang Cai, Ke Ji, Xiang Wan, and 1 others. 2024a. Towards injecting medical visual knowledge into multimodal llms at scale. In *Proceedings of the 2024 conference on empirical methods in natural language processing*, pages 7346–7370.
- Qihui Chen and Yi Hong. 2024. Medblip: Bootstrapping language-image pre-training from 3d medical images and texts. In *Proceedings of the Asian conference on computer vision*, pages 2404–2420.
- Zhe Chen, Jiannan Wu, Wenhai Wang, Weijie Su, Guo Chen, Sen Xing, Muyan Zhong, Qinglong Zhang, Xizhou Zhu, Lewei Lu, and 1 others. 2024b. Internvl: Scaling up vision foundation models and aligning for generic visual-linguistic tasks. In *Proceedings of the IEEE/CVF Conference on Computer Vision and Pattern Recognition*, pages 24185–24198.
- Robert Geirhos, Jörn-Henrik Jacobsen, Claudio Michaelis, Richard Zemel, Wieland Brendel, Matthias Bethge, and Felix A Wichmann. 2020. Shortcut learning in deep neural networks. *Nature Machine Intelligence*, 2(11):665–673.
- Gabriel Grand and Yonatan Belinkov. 2019. Adversarial regularization for visual question answering: Strengths, shortcomings, and side effects. In *Proceedings of the second workshop on shortcomings in vision and language*, pages 1–13.
- Suchin Gururangan, Swabha Swayamdipta, Omer Levy, Roy Schwartz, Samuel Bowman, and Noah A Smith. 2018. Annotation artifacts in natural language inference data. In *Proceedings of the 2018 Conference of the North American Chapter of the Association for Computational Linguistics: Human Language Technologies, Volume 2 (Short Papers)*, pages 107–112.
- Xuehai He, Yichen Zhang, Luntian Mou, Eric Xing, and Pengtao Xie. 2020. Pathvqa: 30000+ questions for medical visual question answering. *arXiv preprint arXiv:2003.10286*.

- Drew A Hudson and Christopher D Manning. 2019. Gqa: A new dataset for real-world visual reasoning and compositional question answering. In *Proceedings of the IEEE/CVF conference on computer vision and pattern recognition*, pages 6700–6709.
- Sumra Khan, Sagar Chhabriya, Aizan Zafar, Sheeraz Arif, Amgad Muneer, Anas Zafar, Shaina Raza, and Rizwan Qureshi. 2026. Towards responsible multi-modal medical reasoning via context-aligned vision-language models. *arXiv preprint arXiv:2604.08815*.
- Jason J Lau, Soumya Gayen, Asma Ben Abacha, and Dina Demner-Fushman. 2018. A dataset of clinically generated visual questions and answers about radiology images. *Scientific data*, 5(1):180251.
- Chunyuan Li, Cliff Wong, Sheng Zhang, Naoto Usuyama, Haotian Liu, Jianwei Yang, Tristan Naumann, Hoifung Poon, and Jianfeng Gao. 2023. Llavamed: Training a large language-and-vision assistant for biomedicine in one day. *Advances in Neural Information Processing Systems*, 36:28541–28564.
- Zujie Liang, Weitao Jiang, Haifeng Hu, and Jiaying Zhu. 2020. Learning to contrast the counterfactual samples for robust visual question answering. In *Proceedings of the 2020 conference on empirical methods in natural language processing (EMNLP)*, pages 3285–3292.
- Bo Liu, Li-Ming Zhan, Li Xu, Lin Ma, Yan Yang, and Xiao-Ming Wu. 2021. Slake: A semantically-labeled knowledge-enhanced dataset for medical visual question answering. In *2021 IEEE 18th international symposium on biomedical imaging (ISBI)*, pages 1650–1654. IEEE.
- Pan Lu, Swaroop Mishra, Tanglin Xia, Liang Qiu, Kai-Wei Chang, Song-Chun Zhu, Oyvind Tafjord, Peter Clark, and Ashwin Kalyan. 2022. Learn to explain: Multimodal reasoning via thought chains for science question answering. *Advances in neural information processing systems*, 35:2507–2521.
- Sarah Müller, Louisa Fay, Lisa M Koch, Sergios Gatidis, Thomas Küstner, and Philipp Berens. 2024. Benchmarking dependence measures to prevent shortcut learning in medical imaging. In *International Workshop on Machine Learning in Medical Imaging*, pages 53–62. Springer.
- Long Ouyang, Jeffrey Wu, Xu Jiang, Diogo Almeida, Carroll Wainwright, Pamela Mishkin, Chong Zhang, Sandhini Agarwal, Katarina Slama, Alex Ray, and 1 others. 2022. Training language models to follow instructions with human feedback. *arXiv preprint arXiv:2203.02155*.
- Letitia Parcalabescu, Albert Gatt, Anette Frank, and Iacer Calixto. 2021. [Seeing past words: Testing the cross-modal capabilities of pretrained V&L models](#). *CoRR*, abs/2012.12352.
- Ramprasaath R Selvaraju, Abhishek Das, Ramakrishna Vedantam, Michael Cogswell, Devi Parikh, and Dhruv Batra. 2016. Grad-cam: Why did you say that? *arXiv preprint arXiv:1611.07450*.
- Zhihong Shao, Peiyi Wang, Qihao Zhu, Runxin Xu, Junxiao Song, Xiao Bi, Haowei Zhang, Mingchuan Zhang, YK Li, Yang Wu, and 1 others. 2024. Deepseekmath: Pushing the limits of mathematical reasoning in open language models. *arXiv preprint arXiv:2402.03300*.
- Ravi Shekhar, Sandro Pezzelle, Yauhen Klimovich, Aurélie Herbelot, Moin Nabi, Enver Sangineto, and Raffaella Bernardi. 2017. [FOIL it! Find One mismatch between Image and Language caption](#). In *Proceedings of the 55th Annual Meeting of the Association for Computational Linguistics (Volume 1: Long Papers)*, pages 255–265, Vancouver, Canada. Association for Computational Linguistics.
- Sasha Sheng, Amanpreet Singh, Vedanuj Goswami, Jose Alberto Lopez Magana, Wojciech Galuba, Devi Parikh, and Douwe Kiela. 2021. [Human-adversarial visual question answering](#). *ArXiv*, abs/2106.02280.
- Zhiqing Sun, Sheng Shen, Shengcao Cao, Haotian Liu, Chunyuan Li, Yikang Shen, Chuang Gan, Liangyan Gui, Yu-Xiong Wang, Yiming Yang, and 1 others. 2024. Aligning large multimodal models with factually augmented rlhf. In *Findings of the Association for Computational Linguistics: ACL 2024*, pages 13088–13110.
- Tristan Thrush, Ryan Jiang, Max Bartolo, Amanpreet Singh, Adina Williams, Douwe Kiela, and Candace Ross. 2022. [Winoground: Probing vision and language models for visio-linguistic compositionality](#). In *Proceedings of the IEEE/CVF Conference on Computer Vision and Pattern Recognition (CVPR)*, pages 5238–5248.
- Miles Turpin, Julian Michael, Ethan Perez, and Sam Bowman. 2023. [Language models don’t always say what they think: Unfaithful explanations in chain-of-thought prompting](#). *ArXiv*, abs/2305.04388.
- U.S. Food and Drug Administration. 2021. [Artificial intelligence/machine learning \(AI/ML\)-based software as a medical device \(SaMD\) action plan](#). Technical report, Center for Devices and Radiological Health, U.S. Food and Drug Administration.
- Jason Wei, Xuezhi Wang, Dale Schuurmans, Maarten Bosma, Brian Ichter, Fei Xia, Ed H. Chi, Quoc V. Le, and Denny Zhou. 2022. Chain-of-thought prompting elicits reasoning in large language models. In *Advances in Neural Information Processing Systems (NeurIPS)*, volume 35, pages 24824–24837.
- Spencer Whitehead, Suzanne Petryk, Vedaad Shakib, Joseph Gonzalez, Trevor Darrell, Anna Rohrbach, and Marcus Rohrbach. 2022. Reliable visual question answering: Abstain rather than answer incorrectly. In *European Conference on Computer Vision*, pages 148–166. Springer.

- Guowei Xu, Peng Jin, Ziang Wu, Hao Li, Yibing Song, Lichao Sun, and Li Yuan. 2025. Llava-cot: Let vision language models reason step-by-step. In *Proceedings of the IEEE/CVF International Conference on Computer Vision*, pages 2087–2098.
- Wen-wai Yim, Yujuan Fu, Asma Ben Abacha, Neal Snider, Thomas Lin, and Meliha Yetisgen. 2023. Acibench: a novel ambient clinical intelligence dataset for benchmarking automatic visit note generation. *Scientific data*, 10(1):586.
- Tianyu Yu, Yuan Yao, Haoye Zhang, Taiwen He, Yifeng Han, Ganqu Cui, Jinyi Hu, Zhiyuan Liu, Hai-Tao Zheng, Maosong Sun, and 1 others. 2024. Rlhf-v: Towards trustworthy mllms via behavior alignment from fine-grained correctional human feedback. In *Proceedings of the IEEE/CVF Conference on Computer Vision and Pattern Recognition*, pages 13807–13816.
- Tianyu Yu, Haoye Zhang, Qiming Li, Qixin Xu, Yuan Yao, Da Chen, Xiaoman Lu, Ganqu Cui, Yunkai Dang, Taiwen He, and 1 others. 2025. Rlaif-v: Open-source ai feedback leads to super gpt-4v trustworthiness. In *Proceedings of the Computer Vision and Pattern Recognition Conference*, pages 19985–19995.
- Mert Yuksekgonul, Federico Bianchi, Pratyusha Kalluri, Dan Jurafsky, and James Zou. 2023. [When and why vision-language models behave like bags-of-words, and what to do about it?](#) In *International Conference on Learning Representations (ICLR)*.
- Anas Zafar, Leema Krishna Murali, and Ashish Vasht. 2026. Beyond accuracy: Evaluating visual grounding in multimodal medical reasoning. *arXiv preprint arXiv:2603.03437*.
- Kai Zhang, Rong Zhou, Eashan Adhikarla, Zhiling Yan, Yixin Liu, Jun Yu, Zhengliang Liu, Xun Chen, Brian D. Davison, Hui Ren, Jing Huang, Chen Chen, Yuyin Zhou, Sunyang Fu, Wei Liu, Tianming Liu, Xiang Li, Yong Chen, Lifang He, and 4 others. 2024. [A generalist vision–language foundation model for diverse biomedical tasks.](#) *Nature Medicine*, 30(11):3129–3141.
- Xiaoman Zhang, Chaoyi Wu, Ziheng Zhao, Weixiong Lin, Ya Zhang, Yanfeng Wang, and Weidi Xie. 2023a. Pmc-vqa: Visual instruction tuning for medical visual question answering. *arXiv preprint arXiv:2305.10415*.
- Zhuosheng Zhang, Aston Zhang, Mu Li, Hai Zhao, George Karypis, and Alex Smola. 2023b. Multi-modal chain-of-thought reasoning in language models. *arXiv preprint arXiv:2302.00923*.
- Yuxin Zuo, Shang Qu, Yifei Li, Zhangren Chen, Xuekai Zhu, Ermo Hua, Kaiyan Zhang, Ning Ding, and Bowen Zhou. 2025. Medxpertqa: Benchmarking expert-level medical reasoning and understanding. *arXiv preprint arXiv:2501.18362*.